$FAPb_{0.5}Sn_{0.5}I_3$, A narrow Bandgap Perovskite Synthesized through Evaporation Methods for Solar Cell Applications

Ana M. Igual-Muñoz, Jorge Ávila, Pablo P. Boix*, and Henk J. Bolink*.

Instituto de Ciencia Molecular, Universidad de Valencia, C/J. Beltran 2, 46980 Paterna, Spain.

*E-mail: Pablo.P.Boix@uv.es; henk.bolink@uv.es

Keywords: perovskite, photovoltaics, tin, lead, vacuum-deposition

Abstract

The tunability of the optoelectrical properties upon compositional modification is a key characteristic of metal halide perovskites. In particular, bandgaps narrower than those in conventional lead-based perovskites are essential to achieve the theoretical efficiency limit of single-absorber solar cells, as well as to develop multi-junction tandem devices. In this study, we report the solvent-free vacuum-deposition of a narrow bandgap perovskite based on tin-lead metal and formamidinium cation. We obtain pinhole-free films with 1.28 eV bandgap by thermal co-deposition of precursors. The optoelectrical quality of these films is demonstrated by their use in solar cells with power conversion efficiency of 13.98%.

Introduction

Halide perovskite-based optoelectronics have become a topic of intense research during the last decade. The excellent properties of this family of materials, such as high optical absorption coefficient and long charge diffusion lengths[1], are particularly interesting for photovoltaic applications, and have attracted the attention of the research community. As a result, their photovoltaic conversion efficiency has increased from 3.8% in 2009 up to 24.2% in 2019. [2–5] The unprecedented evolution of perovskite solar cells' photovoltaic efficiency is currently approaching the theoretical Shockley-Queisser limit, and further efficiency enhancements require a careful analysis of the loses. In that context, achieving perovskite light harvesters with a bandgap close to the optimal one (~1.34 eV) would constitute a promising approach to reduce the losses of single absorber devices. [6–8]

On the other hand, multi-junction solar cells are an alternative strategy to exceed the Shockley-Queisser limit. Multi-junction solar cells use two or more absorbers to maximize the harvesting of the solar spectrum yet minimizing the thermalization losses. This kind of devices can deliver a superior power per area compared to standard single-junction devices, but the use of absorbers with complementary bandgaps is needed to maximize the maximum efficiency. Therefore, perovskites with narrower bandgap than the widely extended $CH_3NH_3PbI_3$ (1.55-1.6 eV) and derivatives are needed to use the full potential of multi-junction solar cells. [9,10]

One of the advantages of halide perovskite semiconductors is the compositional tunability of their optoelectrical properties. [11] Complete or partial substitution of lead (Pb) by tin (Sn) in this kind of perovskites leads to a reduction of the bandgap.[12,13] While replacing Pb with Sn is demonstrated to decrease the bandgap down to 1.1 eV[14–16], the industrial scale synthesis and further commercialization of this perovskites has obstacles, as the easy oxidation of Sn^{2+} and further doping of the perovskites by Sn^{4+}.[17] In recent studies, it has been reported how perovskites based on tin-lead mixtures can enhance the stability of this species, while it allows to tune the bandgap to suitable values for their use as a narrow-bandgap absorber in perovskite-perovskite multijunction solar cells. [18] Moreover, the introduction of the formamidinium ($CH_5N_2^+$, FA^+) cation into the perovskite composition can further reduce the absorption bandgap[19], while improving the thermal stability of the material. [20] Successive optimization of these tin-lead alloyed perovskites has resulted in power conversion efficiencies up to 19.03%. [21,22]

In this work, we study the partial replacement of Pb^{+2} by Sn^{+2} in a $FAPbI_3$ perovskite fabricated by simultaneous thermal vacuum deposition of the precursors. This fabrication technique is solvent-free and intrinsically additive [23], which results in a reduction of the toxicity in the production chain and has the potential to be directly applied to the fabrication of complex multi-layer stacks required in the multi-junction solar cell design. [24] We develop a method to fabricate vacuum deposited $FAPb_{0.5}Sn_{0.5}I_3$ and present the optical, morphological and structural characterization of the resulting films. The targeted composition, 50% Sn 50% Pb, leads to a bandgap of 1.28 eV, similar to what has been previously reported for perovskites prepared using the same starting materials and ratios by solution methods 1.23 eV.[18] These bandgaps are suitable for use in a tandem solar cell with a corresponding wider bandgap sub-cell. [25,26] The films were implemented in solar cells reaching a maximum efficiency close to 14% demonstrating the potential of these films and preparation method.

Discussion

$FAPb_{0.5}Sn_{0.5}I_3$ films were fabricated by simultaneous thermal vacuum deposition of FAI, SnI_2, PbI_2 precursors in an N_2 filled glovebox. A fourth thermal source was used to co-deposit SnF_2 as an additive. The fate of each evaporation source is monitored by an individual microbalance crystal sensor during the sublimation. A scheme of the evaporation chamber is represented in Figure 1.

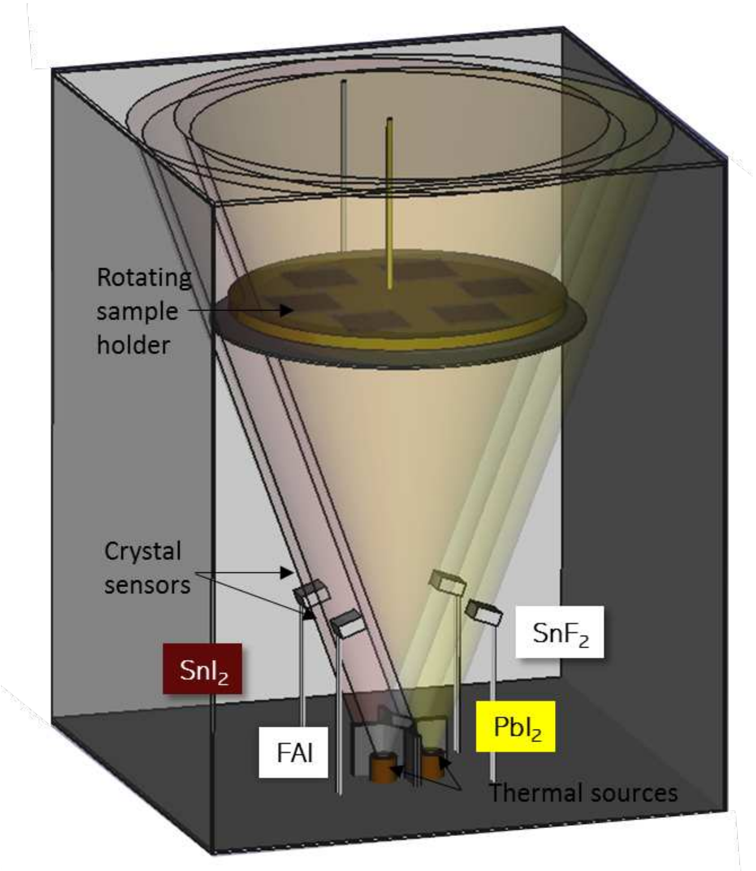

Figure 1. Scheme of the evaporator during the perovskite evaporation including the position for the materials and the different parts of the evaporator.

An independent calibration of each sensor-source was carried out prior to the synthesis of the perovskite in order to establish the proper deposition conditions of the precursors. This calibration was done by depositing a thick (50 to 100 nm) film of each precursor on a glass substrate while simultaneously monitoring the microbalance crystal sensor reading and verifying the indicated thickness by off-line thickness measurement using a mechanical profilometer. In order to avoid the cross-reading of the crystal sensors, the sources are sequentially operated starting from the material that introduces more cross-reading in the other sensors, which is FAI. Afterwards, the temperature of PbI_2 and SnI_2 was increased to obtain the desired rates. Finally, as the rate required for SnF_2 source is significantly lower, it was the last source to be heated. The final rates were obtained by the sum of the rate desired plus the cross-reading on each sensor.

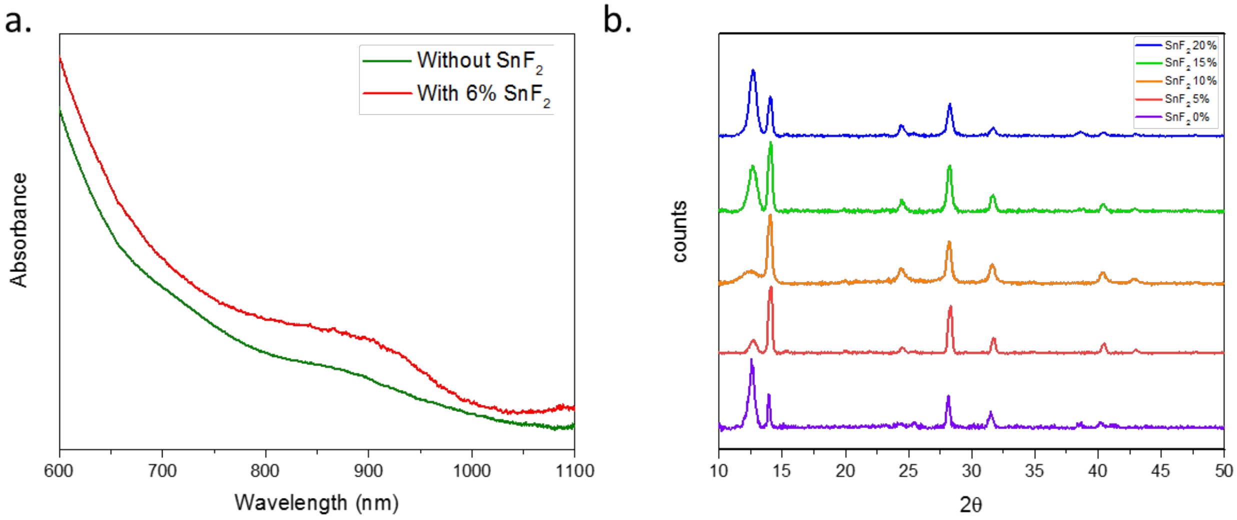

Figure 2. (a) UV-Vis absorbance of $FAPb_{0.5}Sn_{0.5}I_3$ with 6% SnF_2 and without SnF_2. (b) XRD pattern obtained for a $FAPb_{0.5}Sn_{0.5}I_3$ film on PTAA, with different amounts of SnF_2 (percentage related to SnI_2).

The thickness of all the different perovskite films was carefully maintained between 350 nm and 420 nm, showing an accurate thickness control achieved by sublimation methods. The addition of SnF_2 leads to improved film formation, as observed in the absorbance data (Figure 2a).

This point is supported by the crystallinity of the perovskite films, which was studied using XRD in GIXRD setup. The sample prepared without SnF_2 additive displays an XRD pattern with the peaks corresponding to the perovskite are significantly less intense, while the peak at 12.7º, classically ascribed to PbI_2, is the dominant one (Figure 2b). Furthermore, a small peak attributed to SnI_4 may be observed centered at 25.2º. Therefore, the improved film formation upon SnF_2 addition appears as an effect additional to the reduction of the detrimental Sn^{+4} generation, as it was previously reported for Sn-Pb perovskites prepared using a solvent based procedure.[17,27,28] Interestingly, despite the reduction of the peak at 12.7º when small amounts of SnF_2 are added, higher rates of SnF_2 gradually make this diffraction peak more prominent, and generate an additional peak at 38.7º observed for the 20% SnF_2 sample. These signals (12.7º and 38.7º) can be associated to PbI_2 and SnI_2, which suggest that SnF_2 addition induces an excess of these materials in the resulting perovskite film. Similar effect has been reported to have a beneficial impact in the resulting perovskites[29], [30]. The rest of the peaks are consistent with a perovskite containing 50% of Sn and 50 % of Pb, as expected from the rates of deposition.[18,31] Considering a trade-off between the perovskite formation and the metal salts excess, we decided to use the rate of 10% for the subsequent studies. A preliminary evaluation of the stability of these films was carried out by monitoring the evolution of the UV-Vis absorbance of air-exposed films (Figure S1). While there is no significant decay of the perovskite absorption during the initial hours, the degradation is clear after one day, which suggests a decomposition of the film. The ambient effect is also evident when the film conductivity is measured (Figure S2). Under N_2 atmosphere, the perovskite conductivity remains almost unaffected during the explored timeframe. In contrast, the air exposure results in a conductivity enhancement of almost one order of magnitude in few minutes, which is attributed to the Sn^{+4} formation.

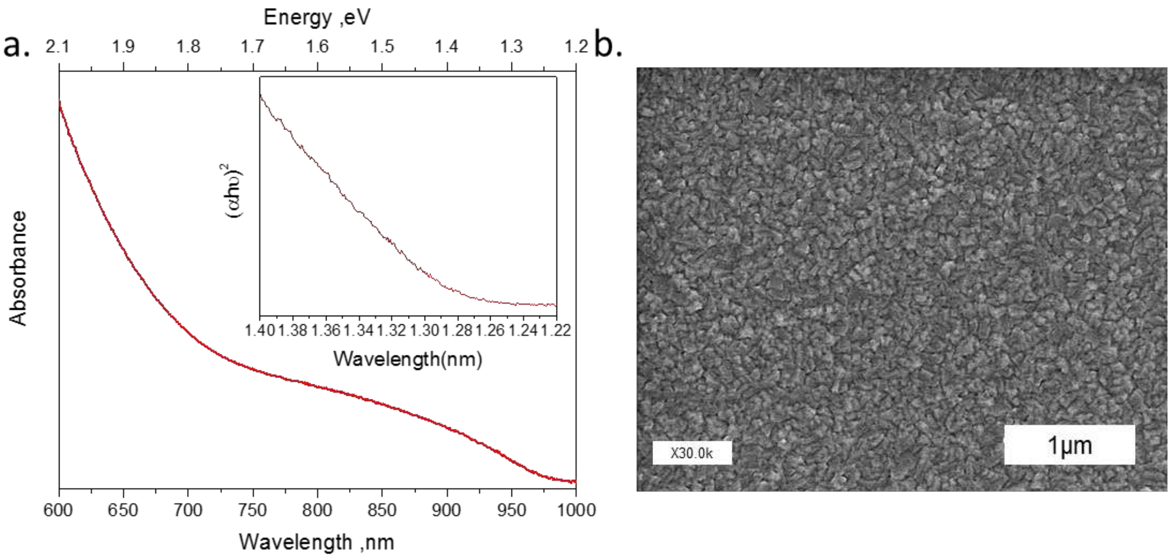

Figure 3. (a) UV-Vis absorbance for a $FAPb_{0.5}Sn_{0.5}I_3$ film with 10% SnF_2 as an additive. Tauc plot calculation from the absorbance in the inset. (b) SEM image for the surface of a $FAPb_{0.5}Sn_{0.5}I_3$ film.

Once deposited onto ambient temperature substrates, the perovskite films were used without further annealing treatment. The absorbance of this perovskite extends up to 970 nm (shown in Figure 3a) according to the Tauc plot corresponding to a direct allowed transition in the bandgap of 1.28 eV (Figure 3a).[32] This value is in line with those obtained from solution-processed perovskites with similar Sn-Pb precursor ratios.[18] The surface of this perovskite thin film can be observed in Figure 3b from a scanning electron microscopy image. This image shows a homogeneous distribution of the grains, sized between 60 and 100 nm. It is worth to mention that vacuum-deposition of perovskites usually results in a smaller grain size than the one obtained by solution-process. However, this is not necessarily limiting the achievable power conversion efficiency of solar cells employing them.[33] More importantly, the SEM top view also displays a smooth pinhole-free surface, crucial to avoid leakage paths in the full device, an encouraging sign of the suitability of vapor-deposition methods for this kind of perovskites. SEM images of samples containing three different quantities of SnF_2 are shown in Figure S3, where no significant morphological differences are observed.

In order to assess the quality of the films, some were employed to fabricate photovoltaic devices with a p-i-n configuration (hole selective material deposited on the incident light side of the device), as detailed in the Experimental Section. The layers that constitute the full stack were ITO/MoO_3/Poly[bis(4-phenyl) (2,4,6-trimethylphenyl) amine] (PTAA)/$FAPb_{0.5}Sn_{0.5}I_3$/fullerene (C_{60})/2,9-Dimethyl-4,7-diphenyl-1,10-phenanthroline (BCP)/Ag, as represented in Figure 4a. The dark current-voltage characteristics of the devices (Figure 4b) show a reduced leakage current and a good diode rectification, suggesting that the formation of Sn^{+4} is effectively suppressed during the fabrication.

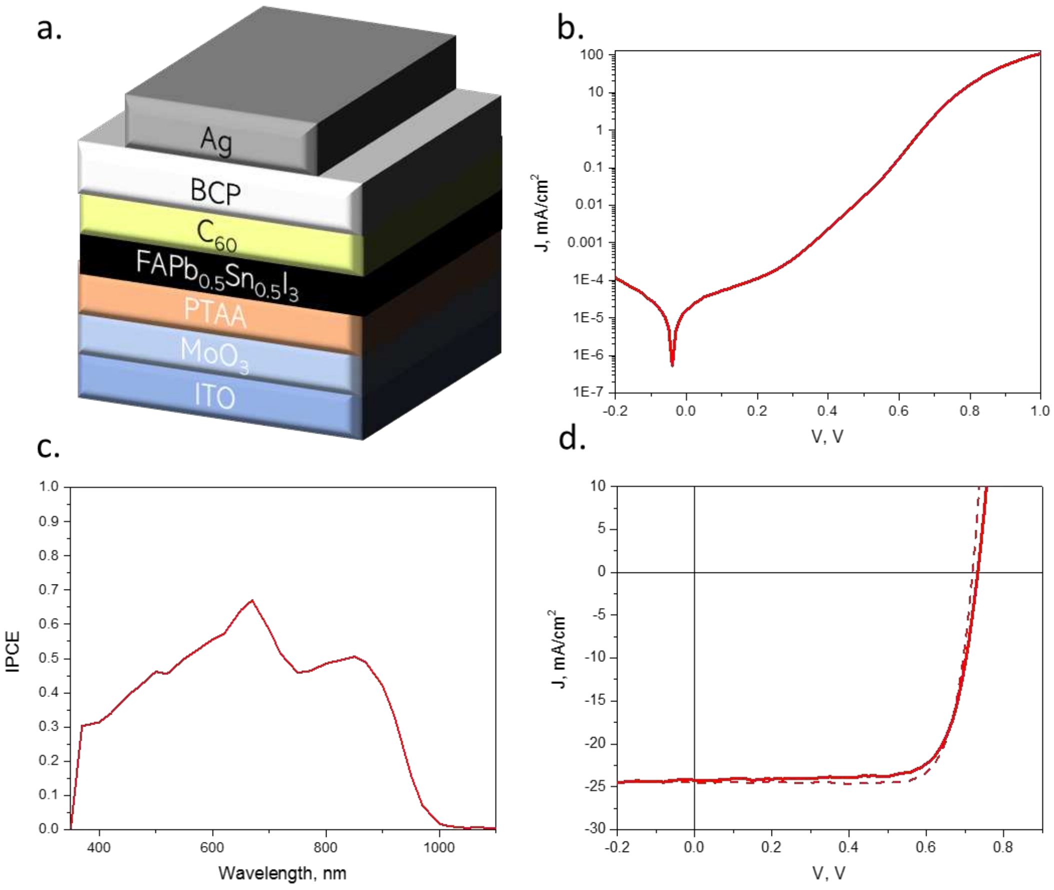

Figure 4. (a) Device structure. (b) J-V characteristics measured in dark conditions for the best performing device. (c) External quantum efficiency of a $FAPb_{0.5}Sn_{0.5}I_3$ solar cell. (d) J-V characteristics under illumination for the best performing device (from positive to negative potential) and solid lines represent forward measurements (from negative to positive potential).

Figure 4c shows the IPCE of the a $FAPb_{0.5}Sn_{0.5}I_3$ solar cell. These devices were synthesized with a thickness of 340 nm, implying that further optimization of the films, including their thickness could increase the current generation in the infrared region of the spectra. Figure 4d displays the current-voltage (*J-V*) characteristics under AM1.5G simulated illumination for the best performing device. Power conversion efficiency achieves a value of 13.98 % in the reverse scan (from V_{OC}, to short circuit, J_{SC}), with V_{OC} of 0.72 V, fill factor (*FF*) of 79.3% and J_{SC} of 24.5 mA cm^{-2}, close to the one obtained from the EQE integration. V_{OC} of 0.73 V, *FF* of 73.3% and J_{SC} of 24.3 mA cm^{-2} are obtained at forward scan (from J_{SC} to $V_{OC)}$, which results in an almost negligible hysteresis.

These results demonstrate the potential of vacuum-deposition for the fabrication of tin-lead perovskite solar cells.

Conclusions

We have developed a method to fabricate $FAPb_{0.5}Sn_{0.5}I_3$ from vacuum-deposition methods. The co-evaporation of the precursors, along with the deposition of SnF_2 additive results in pinhole free homogeneous perovskite films with 60-100 nm grains and a ~1.28 eV bandgap without additional annealing. These films, when integrated in a sandwich type diode structure, show low dark conductivity indicative of the effective suppression of the oxidation of the Sn^{2+} precursor to Sn^{4+}. When illuminated by simulated sun light these diodes have a power conversion efficiency >13% further demonstrating the high quality of the perovskite films. This work opens a new processing route to fabricate narrow-bandgap perovskites by vacuum-deposition, with the potential to achieve the efficiency limit of single-absorber solar cells or to integrate them in multi-junction perovskite tandems upon further optimization.

Experimental Methods

Molybdenum oxide (MoO_3) and bathocuproine (BCP) were obtained from Lumtec, poly(triaryl amine) (PTAA) and C_{60} were obtained from Sigma Aldrich, patterned ITO containing glass substrates were obtained from Naranjo Substrates. The perovskite precursors used in this study were obtained from Tokio Chemical Industries; $PbI_2 > 98\%$ purity, Sigma-Aldrich; $SnF_2 > 99\%$ purity, Cymit (Alfa Aesar); $SnI_2 > 99.999\%$ purity ultradry and Lumtec; FAI > 99.5 %.

To facilitate hole extraction 5 nm of MoO_3 was thermally evaporated at a base pressure of $2x10^{-6}$ mbar on indium tin oxide (ITO) containing substrates. After this, on top of these films a layer, of PTAA was spin-coated at 1500 rpm for 30 s and then thermally annealed at 100ºC for 10 minutes in a nitrogen atmosphere. These ITO/MoO3/PTAA covered substrates were used for the deposition of $FASn_{0.5}Pb_{0.5}I_3$ films following the procedure described below. On top of the perovskite, thin layers of C_{60} and BCP (25 and 8 nm, respectively) were thermally evaporated using a dedicated vacuum chamber with a base pressure of $3x10^{-6}$ mbar. Finally, the films were transferred to a dedicated vacuum chamber used solely for metal deposition where 100 nm of Ag as the top electrode was deposited by thermal evaporation at a pressure of $2x10^{-6}$ mbar. The resulting diodes were then characterized by current voltage sweeps (using a Keithley Model 2400) in the dark and illuminated Incident Photon to Current Efficiency (IPCE) measurements were done by measuring the cell response at different wavelengths obtained with a white halogen lamp combined with band-pass filters. The solar spectrum was corrected by calibration with a Silicon reference cell, previously calibrated (MiniSun simulator by ECN, the Netherlands). The current density voltage (J-V) characteristics were obtained using a solar simulator by Abet Technologies, model 10500 with an AM1.5G xenon lamp as the light source. Keithley 2400 source measure unit and under white light illumination. A shadow mask with an aperture of 0.01 cm^2 was used to prevent illumination of non-active area.

Perovskite film preparation procedure: $FAPb_{0.5}Sn_{0.5}I_3$ films were fabricated by simultaneous thermal vacuum deposition of the precursors FAI, SnI_2, PbI_2 and SnF_2 on ITO/MoO3/PTAA covered substrates at ambient temperature. The evaporation was done in a chamber at a pressure of $3x10^{-6}$ mbar. Four crucibles were filled with the different precursors and evaporated at the following temperatures, which were identified after a study of sublimation rates and final perovskite composition as discussed in the main section of this manuscript: 170 ºC for FAI, 180 ºC for SnI_2, 210 ºC for PbI2 and 145 ºC for SnF_2. The thickness of the films was controlled by the double of the rate of FAI being 0.6 Å s^{-1}. Structural properties were studied using X-Ray Diffraction (XRD). Grazing incident X-ray diffraction (GIXRD) patterns were collected at room temperature on an Empyrean PANanalytical powder diffractometer using the Cu Kα1 radiation. Optical properties were studied using UV-Visible spectroscopy. A fiber optics based Avantes Avaspec2048 Spectrometer was used. Morphological properties were studied using a Scanning electron microscopy (SEM) Hitachi S-4800 microscope at an accelerating voltage of 20 kV. The samples were metallized prior to observation with an Au- Pd coating.

Acknowledgment

The research leading to these results has received funding from the European Union Programme for Research and Innovation Horizon 2020 (2014-2020) under the project INFORM (grant 675867), the Spanish Ministry of Economy and Competitiveness (MINECO) via the Unidad de Excelencia María de Maeztu MDM-2015-0538, MAT2017-88821-R, MAT2017-88905-P and

PCIN-2015-255, and the Generalitat Valenciana (Prometeo/2016/135). H. J. B. acknowledges the support of ERA NET PCIN-2017-014. P.P.B. thanks the MINECO for his post-doctoral RyC contracts. PPB acknowledges the financial support from the Conselleria d'Educació, Investigació, Cultura i Esport Valenciana (SEJI2017/2017/012).

Conflict of Interest

The authors declare no financial or commercial Conflict of Interest.

Bibliography

[1] N. J. Jeon, J. H. Noh, W. S. Yang, Y. C. Kim, S. Ryu, J. Seo, S. Il Seok, *Nature* **2015**, *517*, 476.

[2] A. Kojima, K. Teshima, T. Miyasaka, Y. Shirai, *210th ECS Meet.* **2006**.

[3] N. J. Jeon, H. Na, E. H. Jung, T. Y. Yang, Y. G. Lee, G. Kim, H. W. Shin, S. Il Seok, J. Lee, J. Seo, *Nat. Energy* **2018**, *3*, 682.

[4] Q. Jiang, Y. Zhao, X. Zhang, X. Yang, Y. Chen, Z. Chu, Q. Ye, X. Li, Z. Yin, J. You, *Nat. Photonics* **2019**, *13*, 460.

[5] "NREL," can be found under https://www.nrel.gov/pv/cell-efficiency.html, **2019**.

[6] S. Rühle, *Sol. Energy* **2016**, *130*, 139.

[7] W. Shockley, H. J. Queisser, *J. Appl. Phys.* **1961**, *32*, 510.

[8] Z. Yang, A. Rajagopal, A. K. Y. Jen, *Adv. Mater.* **2017**, *29*, 1704418.

[9] M. Anaya, G. Lozano, M. E. Calvo, H. Míguez, *Joule* **2017**, *1*, 769.

[10] B. Chen, X. Zheng, Y. Bai, N. P. Padture, J. Huang, *Adv. Energy Mater.* **2017**, *7*, 1602400.

[11] W. Li, Z. Wang, F. Deschler, S. Gao, R. H. Friend, A. K. Cheetham, *Nat. Rev. Mater.* **2017**, *2*, 16099.

[12] J. Zhao, L. Wei, C. Jia, H. Tang, X. Su, Y. Ou, Z. Liu, C. Wang, X. Zhao, H. Jin, P. Wang, G. Yu, G. Zhang, J. Liu, *J. Mater. Chem. A* **2018**, *6*, 20224.

[13] Y. Ogomi, A. Morita, S. Tsukamoto, T. Saitho, N. Fujikawa, Q. Shen, T. Toyoda, K. Yoshino, S. S. Pandey, S. Hayase, *J. Phys. Chem. Lett.* **2014**, *5*, 1004.

[14] W. Liao, D. Zhao, Y. Yu, N. Shrestha, K. Ghimire, C. R. Grice, C. Wang, Y. Xiao, A. J. Cimaroli, R. J. Ellingson, N. J. Podraza, K. Zhu, R. G. Xiong, Y. Yan, *J. Am. Chem. Soc.* **2016**, *138*, 12360.

[15] N. K. Noel, S. D. Stranks, A. Abate, C. Wehrenfennig, S. Guarnera, A. A. Haghighirad, A. Sadhanala, G. E. Eperon, S. K. Pathak, M. B. Johnston, A. Petrozza, L. M. Herz, H. J. Snaith, *Energy Environ. Sci.* **2014**, *7*, 3061.

[16] J. Im, C. C. Stoumpos, H. Jin, A. J. Freeman, M. G. Kanatzidis, *J. Phys. Chem. Lett.* **2015**, *6*, 3503.

[17] S. Gupta, D. Cahen, G. Hodes, *J. Phys. Chem. C* **2018**, *122*, 13926.

[18] G. E. Eperon, T. Leijtens, K. A. Bush, R. Prasanna, T. Green, J. T. W. Wang, D. P. McMeekin, G. Volonakis, R. L. Milot, R. May, A. Palmstrom, D. J. Slotcavage, R. A.

Belisle, J. B. Patel, E. S. Parrott, R. J. Sutton, W. Ma, F. Moghadam, B. Conings, A. Babayigit, H. G. Boyen, S. Bent, F. Giustino, L. M. Herz, M. B. Johnston, M. D. McGehee, H. J. Snaith, *Science (80-.).* **2016**, *354*, 861.

[19] T. M. Koh, T. Krishnamoorthy, N. Yantara, C. Shi, W. L. Leong, P. P. Boix, A. C. Grimsdale, S. G. Mhaisalkar, N. Mathews, *J. Mater. Chem. A* **2015**, *3*, 14996.

[20] T. Liu, Y. Zhou, Z. Li, L. Zhang, M. G. Ju, D. Luo, Y. Yang, M. Yang, D. H. Kim, W. Yang, N. P. Padture, M. C. Beard, X. C. Zeng, K. Zhu, Q. Gong, R. Zhu, *Adv. Energy Mater.* **2018**, *8*, 1800232.

[21] G. Kapil, T. S. Ripolles, K. Hamada, Y. Ogomi, T. Bessho, T. Kinoshita, J. Chantana, K. Yoshino, Q. Shen, T. Toyoda, T. Minemoto, T. N. Murakami, H. Segawa, S. Hayase, *Nano Lett.* **2018**, *18*, 3600.

[22] C. Li, Z. Song, D. Zhao, C. Xiao, B. Subedi, N. Shrestha, M. M. Junda, C. Wang, C. S. Jiang, M. Al-Jassim, R. J. Ellingson, N. J. Podraza, K. Zhu, Y. Yan, *Adv. Energy Mater.* **2019**, *9*, 1803135.

[23] J. Ávila, C. Momblona, P. P. Boix, M. Sessolo, H. J. Bolink, *Joule* **2017**, *1*, 431.

[24] J. Ávila, C. Momblona, P. Boix, M. Sessolo, M. Anaya, G. Lozano, K. Vandewal, H. Míguez, H. J. Bolink, *Energy Environ. Sci.* **2018**, *11*, 3292.

[25] D. Zhao, C. Chen, C. Wang, M. M. Junda, Z. Song, C. R. Grice, Y. Yu, C. Li, B. Subedi, N. J. Podraza, X. Zhao, G. Fang, R. G. Xiong, K. Zhu, Y. Yan, *Nat. Energy* **2018**, *3*, 1093.

[26] D. Zhao, Y. Yu, C. Wang, W. Liao, N. Shrestha, C. R. Grice, A. J. Cimaroli, L. Guan, R. J.

Ellingson, K. Zhu, X. Zhao, R. G. Xiong, Y. Yan, *Nat. Energy* **2017**, *2*, 17018.

[27] I. Chung, B. Lee, J. He, R. P. H. Chang, M. G. Kanatzidis, *Nature* **2012**, *485*, 486.

[28] M. H. Kumar, S. Dharani, W. L. Leong, P. P. Boix, R. R. Prabhakar, T. Baikie, C. Shi, H. Ding, R. Ramesh, M. Asta, M. Graetzel, S. G. Mhaisalkar, N. Mathews, *Adv. Mater.* **2014**, *26*, 7122.

[29] D. P. McMeekin, S. Mahesh, N. K. Noel, M. T. Klug, J. C. Lim, J. H. Warby, J. M. Ball, L. M. Herz, M. B. Johnston, H. J. Snaith, *Joule* **2019**, *3*, 387.

[30] D. Ramirez, K. Schutt, Z. Wang, A. J. Pearson, E. Ruggeri, H. J. Snaith, S. D. Stranks, F. Jaramillo, *ACS Energy Lett.* **2018**, *3*, 2246.

[31] W. Wang, D. Zhao, F. Zhang, L. Li, M. Du, C. Wang, Y. Yu, Q. Huang, M. Zhang, L. Li, J. Miao, Z. Lou, G. Shen, Y. Fang, Y. Yan, *Adv. Funct. Mater.* **2017**, *27*, 1703953.

[32] J. Tauc, R. Grigorovici, A. Vancu, *Phys. Status Solidi* **1966**, *15*, 627.

[33] C. Momblona, L. Gil-Escrig, E. Bandiello, E. M. Hutter, M. Sessolo, K. Lederer, J. Blochwitz-Nimoth, H. J. Bolink, *Energy Environ. Sci.* **2016**, *9*, 3456.